International Journal of Solids and Structures 46 (2009) 2950–2958

Contents lists available at ScienceDirect

International Journal of Solids and Structures

journal homepage: www.elsevier.com/locate/ijsolstr

Transient response of a magnetoelectroelastic solid with two collinear dielectric cracks under impacts

Xian-Ci Zhong [a], Fang Liu [a], Xian-Fang Li [b,*]

[a] School of Mathematics and Information Science, Guangxi University, Nanning, Guangxi 530004, China
[b] Institute of Mechanics and Sensor Technology, School of Civil Engineering and Architecture, Central South University, Changsha, Hunan 410083, China

ARTICLE INFO

Article history:
Received 4 January 2009
Received in revised form 23 February 2009
Available online 5 April 2009

Keywords:
Magnetoelectric solid
Transient analysis
Dielectric crack
Semi-permeable condition
Dynamic intensity factor

ABSTRACT

Dynamic analysis of two collinear electro-magnetically dielectric cracks in a piezoelectromagnetic material is made under in-plane magneto-electro-mechanical impacts. Generalized semi-permeable crack-face boundary conditions are proposed to simulate realistic opening cracks with dielectric. Ideal boundary conditions of a combination of electrically permeable or impermeable and magnetically permeable or impermeable assumptions are several limiting cases of the semi-permeable dielectric crack. Utilizing the Laplace and Fourier transforms, the mixed initial-boundary-value problem is reduced to solving singular integral equations with Cauchy kernel. Dynamic intensity factors of stress, electric displacement, magnetic induction and crack opening displacement (COD) near the inner and outer crack tips are determined in the Laplace transform domain. Numerical results for a special magnetoelectroelastic solid are calculated to show the influences of the dielectric permittivity and magnetic permeability inside the cracks on the crack-face electric displacement and magnetic induction. By means of a numerical inversion of the Laplace transform, the variations of the normalized intensity factors of stress and COD are discussed against applied magnetoelectric impact loadings and the geometry of the cracks for fully impermeable, vacuum, fully permeable cracks and shown in graphics.

1. Introduction

Multiferroic magnetoelectric materials involving both ferroelectric and ferromagnetic phases exhibit the coupling magneto-electro-mechanical effects (Zheng et al., 2004), and have attracted increasing interest due to their promising applications as smart devices (Nan et al., 2008). Due to brittleness of magnetoelectroelastic solids, a considerable number of researchers have focused their attention on fracture analysis under different applied loadings. There are lots of papers published which treat static crack problems of magneto-electroelastic materials such as Wang et al. (2008), Zhao et al. (2007), Zhong and Li (2007), Hu and Li (2005a), Tian and Rajapakse (2005), Gao et al. (2004), Sih et al. (2003) and Liu et al. (2001). Moreover, considering that multifunctional devices work always under dynamic conditions, an investigation of dynamic behavior of magnetoelectroelastic materials weakened by a crack is requisite to understand the reliability of piezoelectromagnetic structures. Along this line, Feng and Pan (2008) investigated the anti-plane dynamic problem of an internal interfacial crack between two dissimilar magnetoelectroelastic plates. For the problems of anti-plane moving crack with constant velocity in a rectangular magnetoelectroelastic body, infinite magnetoelectroelastic material, and the interface of two dissimilar magnetoelectroelastic materials, Hu and his co-workers (2005b, 2006, 2007) studied the singular magneto-electro-elastic field near the crack tip and the branch of crack, respectively. Su et al. (2007) dealt with the interface multi-cracks problem between dissimilar magnetoelectroelastic strips under out-of-plane mechanical and in-plane magneto-electrical impacts. The dynamic response of a magnetoelectroelastic strip with a crack normal to the edges was investigated by Yong and Zhou (2007). By using general crack-face magnetoelectric boundary conditions, the problem of Yoffe type moving interface crack between two dissimilar magnetoelectroelastic materials was solved by Zhong and Li (2006). Li (2005) treated the dynamic problem for a magnetoelectroelastic material with a crack under anti-plane mechanical and in-plane electric and magnetic impacts. The diffraction of anti-plane waves by a single piezoelectric cylindrical inhomogeneity partially bonded to an unbounded piezomagnetic matrix was considered by Du et al. (2004). Zhou et al. (2005) addressed the dynamic analysis of two collinear cracks between two dissimilar magneto-electroelastic materials subjected to anti-plane shear waves. For the problem of inplane magneto-electro-mechanical impact response, Feng et al. (2007) analyzed the dynamic magnetoelectroelastic behavior of a piezoelectromagnetic layer with a penny-shaped crack. Zhong et al. (2009) studied the transient response of magnetoelectroelastic field of a cracked magnetoelectric material subjected to in-plane sudden impacts.

* Corresponding author.
E-mail address: xfli@mail.csu.edu.cn (X.-F. Li).

0020-7683/$ - see front matter © 2009 Elsevier Ltd. All rights reserved.
doi:10.1016/j.ijsolstr.2009.03.023

The above-mentioned works are based on the following four ideal crack-face boundary conditions. That is, electro-magnetically permeable, electro-magnetically impermeable, electrically impermeable and magnetically permeable, electrically permeable and magnetically impermeable are always assumed. However, a realistic crack is full of dielectric inside the crack, which is permeable to electric and magnetic fields. On the other hand, when a crack opens, the crack interior in turn affects the crack opening displacement. Therefore, a more suitable assumption is so-called semi-permeable assumption, which was firstly by Hao and Shen (1994) in analyzing the electroelastic field of piezoelectric materials weakened by an opening crack, and has been verified by experimental observations (Schneider et al., 2003) and by theoretical approach with the finite element analysis (McMeeking, 1999). In fact, four ideal crack-face boundary conditions are the limiting ones of the semi-permeable assumption (Wang and Mai, 2007). Recently, the semi-permeable condition has been extended by Zhong and Li (2007) to solve static opening crack problems of magnetoelectroelastic solids as follows:

$$D^c = -\varepsilon^c \frac{\Delta\phi}{\Delta u_z}, \quad B^c = -\mu^c \frac{\Delta\varphi}{\Delta u_z}, \tag{1}$$

where $\varepsilon^c = \varepsilon_r\varepsilon_0(\varepsilon_0 = 8.85 \times 10^{-12}\ \mathrm{F/m})$ and $\mu^c = \mu_r\mu_0(\mu_0 = 1.26\times 10^{-6}\ \mathrm{Ns^2/C^2})$ are the dielectric permittivity and magnetic permeability of crack interior, respectively; $\Delta\phi$, $\Delta\varphi$ and Δu_z are the jumps of electric potential, magnetic potential and crack opening displacement across the crack, respectively. Note that electric displacement and magnetic induction are nonlinearly dependent on the crack opening displacement. Although the semi-permeable conditions have been applied to treat static crack problems, dynamic analysis of magnetoelectroelastic materials with cracks according to the above-stated crack-face boundary condition is still lacked.

The purpose of the present paper is to investigate the dynamic response of a magnetoelectroelastic solid with two collinear opening cracks by using the semi-permeable magnetoelectric boundary conditions (1). Under the action of inplane magneto-electro-mechanical impact loadings, the mixed initial-boundary-value problem is reduced to solving singular integral equations with Cauchy kernel by applying the Laplace and Fourier transforms. Furthermore, the dynamic intensity factors of stress, electric displacement, magnetic induction and the crack opening displacement are obtained in the Laplace transform domain. Making use of an inversion of the Laplace transform, numerical results are calculated to show the influences of the dielectric permittivity and magnetic permeability inside the cracks, applied magnetoelectric impact loadings and the geometry of the cracks on the physical quantities of concern and shown graphically.

2. Problem and basic equations

Consider a transversely isotropic magnetoelectroelastic solid with two collinear electro-magnetically dielectric cracks as shown in Fig. 1, where Cartesian coordinate system xoz is used with the poling axis as the z-axis. It is assumed that the cracks are situated at the segment of $a < |x| < c$ at the x-axis, and half length of the cracks is $a_0 = (c-a)/2$. For convenience, let us further write $c_0 = (a+c)/2$. Applied magnetic, electric and mechanical impact loadings: $B_0H(t)$, $D_0H(t)$ and $\sigma_0H(t)$ are imposed on the crack surfaces, where B_0, D_0 and σ_0 are constants, and $H(t)$ denotes the Heaviside step function. A dielectric with the electric permittivity ε^c and magnetic permeability μ^c is full of the opening crack interiors. Under the assumption of plane deformation, the constitutive equations based on the linearly magnetoelectroelastic theory can be stated as follows:

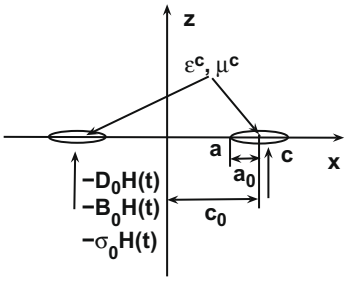

Fig. 1. Two collinear electro-magnetically dielectric cracks embedded in a magnetoelectroelastic solid subjected to in-plane magneto-electro-mechanical impacts.

$$\begin{bmatrix}\sigma_{xx}\\ \sigma_{zz}\\ D_z\\ B_z\end{bmatrix} = \begin{bmatrix}c_{11} & c_{13} & -e_{31} & -h_{31}\\ c_{13} & c_{33} & -e_{33} & -h_{33}\\ e_{31} & e_{33} & \varepsilon_{33} & d_{33}\\ h_{31} & h_{33} & d_{33} & \mu_{33}\end{bmatrix}\begin{bmatrix}\epsilon_{xx}\\ \epsilon_{zz}\\ E_z\\ H_z\end{bmatrix}, \tag{2}$$

$$\begin{bmatrix}\sigma_{xz}\\ D_x\\ B_x\end{bmatrix} = \begin{bmatrix}2c_{44} & -e_{15} & -h_{15}\\ 2e_{15} & \varepsilon_{11} & d_{11}\\ 2h_{15} & d_{11} & \mu_{11}\end{bmatrix}\begin{bmatrix}\epsilon_{xz}\\ E_x\\ H_x\end{bmatrix}, \tag{3}$$

where σ_{ij}, ϵ_{ij}, E_i, D_i, H_i and B_i are the components of stress, strain, electric field, electric displacement, magnetic field and magnetic induction, respectively; e_{kl}, h_{kl} and d_{kl} are the piezoelectric, piezomagnetic and magnetoelectric coupling constants, respectively; c_{kl}, ε_{kl} and μ_{kl} are the elastic stiffness, the dielectric permittivities and the magnetic permeabilities, respectively. Furthermore, the components of strain, electric and magnetic field can be determined by the non-vanishing elastic displacements $u_x(x,z,t)$ and $u_z(x,z,t)$, electric potential $\phi(x,z,t)$ and magnetic potential $\varphi(x,z,t)$, respectively, i.e.

$$\epsilon_{ij} = \frac{1}{2}(u_{i,j} + u_{j,i}), \quad E_i = -\phi_{,i}, \quad H_i = -\varphi_{,i}, \tag{4}$$

where a comma denotes partial differentiation with respect to the suffixed space variable. From the equations of motion, and the equilibrium equations of electric displacements and magnetic inductions, the elastic displacements, electric and magnetic potentials satisfy the basic governing equations

$$c_{11}u_{x,xx} + c_{44}u_{x,zz} + (c_{13}+c_{44})u_{z,xz} + (e_{31}+e_{15})\phi_{,xz} + (h_{31}+h_{15})\varphi_{,xz} = \rho u_{x,tt}, \tag{5}$$

$$c_{44}u_{z,xx} + c_{33}u_{z,zz} + (c_{13}+c_{44})u_{x,xz} + e_{15}\phi_{,xx} + e_{33}\phi_{,zz} + h_{15}\varphi_{,xx} + h_{33}\varphi_{,zz} = \rho u_{z,tt}, \tag{6}$$

$$e_{15}u_{z,xx} + e_{33}u_{z,zz} + (e_{31}+e_{15})u_{x,xz} - \varepsilon_{11}\phi_{,xx} - \varepsilon_{33}\phi_{,zz} - d_{11}\varphi_{,xx} - d_{33}\varphi_{,zz} = 0, \tag{7}$$

$$h_{15}u_{z,xx} + h_{33}u_{z,zz} + (h_{31}+h_{15})u_{x,xz} - d_{11}\phi_{,xx} - d_{33}\phi_{,zz} - \mu_{11}\varphi_{,xx} - \mu_{33}\varphi_{,zz} = 0, \tag{8}$$

where ρ is the mass density. The body forces, free charges, and current densities have been neglected in the present study.

As shown in Fig. 1, due to the symmetry of the problem in geometry and material for two collinear cracks of equal length embedded in a magnetoelectroelastic solid with the poling direction perpendicular to the crack plane, it is reasonable to conclude that the electroelastic field as well as the electro-magnetic field inside the two cracks is symmetric when applied loading is symmetric. For this reason, it is sufficient to investigate the dynamic magnetoelectroelastic field in the region of $x > 0$ and $z > 0$. Fur-

thermore, considering the fact of crack opening, the crack-face boundary conditions in the present study can be written as:

$$\sigma_{zz}(x,0,t) = -\sigma_0 H(t), \quad a < x < c, \ \ t > 0, \tag{9}$$

$$D_z(x,0,t) = -(D_0 - D_0^c)H(t), \quad a < x < c, \ \ t > 0, \tag{10}$$

$$B_z(x,0,t) = -(B_0 - B_0^c)H(t), \quad a < x < c, \ \ t > 0, \tag{11}$$

where

$$D_0^c H(t) = -\varepsilon_r \varepsilon_0 \frac{\Delta\phi(x,0,t)}{\Delta u_z(x,0,t)}, \quad B_0^c H(t) = -\mu_r \mu_0 \frac{\Delta\varphi(x,0,t)}{\Delta u_z(x,0,t)}. \tag{12}$$

Similar to the discussions given by Zhong and Li (2007), it is found that the crack reduces to a so-called vacuum or air crack when $\varepsilon_r = 1$ and $\mu_r = 1$. When $\varepsilon_r = \mu_r = 0$, the crack is an electro-magnetically impermeable one, and when $\varepsilon_r \to \infty$ and $\mu_r \to \infty$, the crack is called as electro-magnetically permeable one. Also, when $\varepsilon_r \to \infty$ and $\mu_r = 0$, the crack is corresponding to an electrically permeable and magnetically impermeable one, and when $\varepsilon_r = 0$, and $\mu_r \to \infty$, the crack leads to an electrically impermeable and magnetically permeable one. Moreover, it is easily shown that D_0^c and B_0^c are independent of the time t, so the time factor $H(t)$ has been extracted in the above.

In addition, applying the continuity of the elastic displacement, electric potential and magnetic potential along the crack-free parts of x-axis and free stress, the boundary conditions read

$$u_z(x,0,t) = 0, \quad 0 < x < a, \ \ c < x < +\infty, \ \ t > 0, \tag{13}$$

$$\phi(x,0,t) = 0, \quad 0 < x < a, \ \ c < x < +\infty, \ \ t > 0, \tag{14}$$

$$\varphi(x,0,t) = 0, \quad 0 < x < a, \ \ c < x < +\infty, \ \ t > 0, \tag{15}$$

$$\sigma_{xz}(x,0,t) = 0, \quad 0 < x < +\infty, \ \ t > 0. \tag{16}$$

3. Singular integral equations

In order to solve the above stated problem, it is natural to assume that the cracked magnetoelectroelastic material is initially at rest and subjected to the following initial conditions:

$$u_x(x,z,0) = 0, \quad \left.\frac{\partial u_x(x,z,t)}{\partial t}\right|_{t=0} = 0, \tag{17}$$

$$u_z(x,z,0) = 0, \quad \left.\frac{\partial u_z(x,z,t)}{\partial t}\right|_{t=0} = 0. \tag{18}$$

Then application of the Laplace transform

$$f^*(p) = \int_0^\infty f(t)\exp(-pt)\,dt, \tag{19}$$

together with (17) and (18) to (5)–(8) leads to

$$c_{11}u^*_{x,xx} + c_{44}u^*_{x,zz} + (c_{13}+c_{44})u^*_{z,xz} + (e_{31}+e_{15})\phi^*_{,xz} + (h_{31}+h_{15})\varphi^*_{,xz} = \rho p^2 u^*_x, \tag{20}$$

$$c_{44}u^*_{z,xx} + c_{33}u^*_{z,zz} + (c_{13}+c_{44})u^*_{x,xz} + e_{15}\phi^*_{,xx} + e_{33}\phi^*_{,zz} + h_{15}\varphi^*_{,xx} + h_{33}\varphi^*_{,zz} = \rho p^2 u^*_z, \tag{21}$$

$$e_{15}u^*_{z,xx} + e_{33}u^*_{z,zz} + (e_{31}+e_{15})u^*_{x,xz} - \varepsilon_{11}\phi^*_{,xx} - \varepsilon_{33}\phi^*_{,zz} - d_{11}\varphi^*_{,xx} - d_{33}\varphi^*_{,zz} = 0, \tag{22}$$

$$h_{15}u^*_{z,xx} + h_{33}u^*_{z,zz} + (h_{31}+h_{15})u^*_{x,xz} - d_{11}\phi^*_{,xx} - d_{33}\phi^*_{,zz} - \mu_{11}\varphi^*_{,xx} - \mu_{33}\varphi^*_{,zz} = 0. \tag{23}$$

Moreover, the Fourier transform technique is further utilized to express the solutions of elastic displacements, electric potential and magnetic potential in Eqs. (20)–(23) as follows:

$$\begin{bmatrix} u_x^*(x,z,p) \\ u_z^*(x,z,p) \\ \phi^*(x,z,p) \\ \varphi^*(x,z,p) \end{bmatrix} = \sum_{j=1}^{4}\int_0^\infty A_j(\xi,p)\exp[-\alpha_j(\xi,p)z] \begin{bmatrix} \sin(\xi x) \\ \eta_{3j}\alpha_j(\xi,p)\cos(\xi x) \\ \eta_{4j}\alpha_j(\xi,p)\cos(\xi x) \\ \eta_{5j}\alpha_j(\xi,p)\cos(\xi x) \end{bmatrix} d\xi, \tag{24}$$

where $\alpha_j(\xi,p)$, η_{3j}, η_{4j} and η_{5j} are given in Appendix A, and $A_j(\xi,p)$ $(j = 1,2,\ldots,8)$ are the unknown functions to be solved. To this end, if applying the Laplace transform (19) to Eqs. (2) and (3), the components of stress, electric displacement, magnetic induction can be obtained in the Laplace transform domain from (24). For example, we have

$$\begin{bmatrix} \sigma_{xz}^*(x,z,p) \\ \sigma_{zz}^*(x,z,p) \\ D_z^*(x,z,p) \\ B_z^*(x,z,p) \end{bmatrix} = -\sum_{j=1}^{4}\int_0^\infty A_j(\xi,p)\exp[-\alpha_j(\xi,p)z] \begin{bmatrix} \beta_{0j}\sin(\xi x) \\ \beta_{1j}\cos(\xi x) \\ \beta_{2j}\cos(\xi x) \\ \beta_{3j}\cos(\xi x) \end{bmatrix} d\xi, \tag{25}$$

where $\beta_{\kappa j}$ $(\kappa = 0,1,2,3)$ are shown in Appendix A.

In what follows, let us focus our attention on seeking the solutions of $A_j(\xi,p)$. Using the Laplace transform (19), the boundary conditions (9)–(11) and (13)–(16) can be rewritten as:

$$\sigma_{zz}^*(x,0,p) = -\frac{\sigma_0}{p}, \quad D_z^*(x,0,p) = -\frac{D_0 - D_0^c}{p}, \quad B_z^*(x,0,p) = -\frac{B_0 - B_0^c}{p}, \quad a < x < c, \tag{26}$$

$$u_z^*(x,0,p) = 0, \quad \phi^*(x,0,p) = 0, \quad \varphi^*(x,0,p) = 0, \quad 0 < x < a, c < x < +\infty, \tag{27}$$

$$\sigma_{xz}^*(x,0,p) = 0, \quad 0 < x < +\infty. \tag{28}$$

From (28), it is found that

$$\sum_{j=0}^{4}\beta_{0j}A_j(\xi,p) = 0. \tag{29}$$

On the other hand, defining generalized dislocation density functions as

$$\begin{bmatrix} g_1(x,p) \\ g_2(x,p) \\ g_3(x,p) \end{bmatrix} = \frac{\partial}{\partial x}\begin{bmatrix} u_z^*(x,0,p) \\ \phi^*(x,0,p) \\ \varphi^*(x,0,p) \end{bmatrix}, \tag{30}$$

and making use of the Fourier inverse transform, from (27) we have

$$\sum_{j=1}^{4}\begin{bmatrix} \eta_{3j} \\ \eta_{4j} \\ \eta_{5j} \end{bmatrix}\alpha_j(\xi,p)A_j(\xi,p) = -\frac{2}{\pi\xi}\int_a^c \begin{bmatrix} g_1(s,p) \\ g_2(s,p) \\ g_3(s,p) \end{bmatrix}\sin(s\xi)\,ds. \tag{31}$$

According to (29) and (31), the expressions of $A_j(\xi,p)$ can be obtained as:

$$\begin{bmatrix} A_1(\xi,p) \\ A_2(\xi,p) \\ A_3(\xi,p) \\ A_4(\xi,p) \end{bmatrix} = [b_{ji}]_{4\times4}\cdot\frac{-2}{\pi\xi}\int_a^c \begin{bmatrix} g_1(s,p) \\ g_2(s,p) \\ g_3(s,p) \\ 0 \end{bmatrix}\sin(s\xi)\,ds, \tag{32}$$

with

$$[b_{ji}]_{4\times4} = \begin{bmatrix} \eta_{31}\alpha_1 & \eta_{32}\alpha_2 & \eta_{33}\alpha_3 & \eta_{34}\alpha_4 \\ \eta_{41}\alpha_1 & \eta_{42}\alpha_2 & \eta_{43}\alpha_3 & \eta_{44}\alpha_4 \\ \eta_{51}\alpha_1 & \eta_{52}\alpha_2 & \eta_{53}\alpha_3 & \eta_{54}\alpha_4 \\ \beta_{01} & \beta_{02} & \beta_{03} & \beta_{04} \end{bmatrix}^{-1}, \tag{33}$$

where "−1" stands for the inverse matrix.

Substituting (32) into (25), from (26) one can obtain

$$\frac{2}{\pi}\int_a^c\int_0^\infty \frac{1}{\xi}\sum_{i=1}^{3}\sum_{j=1}^{4} b_{ji}g_i(s,p)\begin{bmatrix}\beta_{1j}\\ \beta_{2j}\\ \beta_{3j}\end{bmatrix}\sin(s\xi)\cos(x\xi)\,d\xi\,ds = -\frac{1}{p}\begin{bmatrix}\sigma_0\\ D_0-D_0^c\\ B_0-B_0^c\end{bmatrix}, \quad a<x<c. \tag{34}$$

For convenience, introduce the following limit:

$$\lim_{\xi\to\infty}\frac{\sum_{j=1}^{4} b_{ji}\beta_{kj}}{\xi} = r_{ki}, \quad k,i=1,2,3, \tag{35}$$

where r_{ki} are constants dependent on the material properties. With the known result

$$\frac{2}{\pi}\int_0^\infty \cos(x\xi)\sin(s\xi)\,d\xi = \frac{1}{\pi}\left(\frac{1}{s+x}+\frac{1}{s-x}\right), \tag{36}$$

three singular integral equations can be derived from (34) and take the form

$$\frac{1}{\pi}\int_a^c \frac{1}{s-x}\sum_{i=1}^{3}\begin{bmatrix}r_{1i}g_i(s,p)\\ r_{2i}g_i(s,p)\\ r_{3i}g_i(s,p)\end{bmatrix}ds + \frac{1}{\pi}\int_a^c \sum_{i=1}^{3}\begin{bmatrix}K_{1i}(s,x,p)g_i(s,p)\\ K_{2i}(s,x,p)g_i(s,p)\\ K_{3i}(s,x,p)g_i(s,p)\end{bmatrix}ds = -\frac{1}{p}\begin{bmatrix}\sigma_0\\ D_0-D_0^c\\ B_0-B_0^c\end{bmatrix}, \tag{37}$$

where $a<x<c$ and

$$K_{ki}(s,x,p) = 2\int_0^\infty\left[\frac{\sum_{j=1}^{4} b_{ji}\beta_{kj}}{\xi}-r_{ki}\right]\sin(s\xi)\cos(x\xi)\,d\xi + \frac{r_{ki}}{s+x}, \quad k,i=1,2,3. \tag{38}$$

It seems that Eq. (37) cannot be solved analytically because of the complexity of the kernels $K_{ki}(s,x,p)$. In what follows, the Lobatto–Chebyshev collocation method (Theocaris and Ioakimidis, 1977) is used to solve the above singular integral equations with Cauchy kernel numerically. In order to carry out numerical computation, on making use of the following variable transformations:

$$x = \frac{a+c}{2}+\frac{c-a}{2}\bar{x}, \quad s = \frac{a+c}{2}+\frac{c-a}{2}\bar{s}, \quad g_i(s,p) = \frac{f_i(\bar{s},p)}{p}, \quad i=1,2,3, \tag{39}$$

the singular integral equation (37) can be further rewritten as

$$\frac{1}{\pi}\int_{-1}^{1}\frac{1}{\bar{s}-\bar{x}}\sum_{i=1}^{3}\begin{bmatrix}r_{1i}f_i(\bar{s},p)\\ r_{2i}f_i(\bar{s},p)\\ r_{3i}f_i(\bar{s},p)\end{bmatrix}d\bar{s} + \frac{1}{\pi}\int_{-1}^{1}\sum_{i=1}^{3}\begin{bmatrix}\overline{K}_{1i}(\bar{s},\bar{x},p)f_i(\bar{s},p)\\ \overline{K}_{2i}(\bar{s},\bar{x},p)f_i(\bar{s},p)\\ \overline{K}_{3i}(\bar{s},\bar{x},p)f_i(\bar{s},p)\end{bmatrix}d\bar{s} = -\begin{bmatrix}\sigma_0\\ D_0-D_0^c\\ B_0-B_0^c\end{bmatrix}, \quad |\bar{x}|<1, \tag{40}$$

where

$$\overline{K}_{ki}(\bar{s},\bar{x},p) = a_0K_{ki}(a_0\bar{s},a_0\bar{x},p), \quad k,i=1,2,3. \tag{41}$$

Owing to the inverse-square root singularity of the physical quantities at the crack tips, it is convenient to take

$$f_i(\bar{s},p) = \frac{1}{\sqrt{1-\bar{s}^2}}y_i(\bar{s},p), \quad i=1,2,3, \tag{42}$$

where $y_i(\bar{s},p)$ are bounded continuous functions in the interval $|\bar{s}|\leqslant 1$. Consequently, by means of the Lobatto–Chebyshev collocation method, we have

$$\frac{1}{\pi}\int_{-1}^{1}\frac{1}{\bar{s}-\bar{x}}\frac{y_i(\bar{s},p)}{\sqrt{1-\bar{s}^2}}d\bar{s} \approx \frac{1}{n}\sum_{l=0}^{n}\lambda_l\frac{y_i(\bar{s}_l,p)}{\bar{s}_l-\bar{x}_m}, \quad i=1,2,3, \tag{43}$$

where

$$\bar{x}_m = \cos[(2m-1)\pi/(2n)], \quad m=1,2,\ldots,n, \quad \bar{s}_l = \cos(l\pi/n), \quad l=0,1,2,\ldots,n, \quad \lambda_0=\lambda_n=1/2, \quad \lambda_1=\cdots=\lambda_{n-1}=1. \tag{44}$$

Furthermore, Eq. (40) can be expressed as the following discretized versions:

$$\frac{1}{n}\sum_{l=0}^{n}\frac{\lambda_l}{\bar{s}_l-\bar{x}_m}\sum_{i=1}^{3}\begin{bmatrix}r_{1i}y_i(\bar{s}_l,p)\\ r_{2i}y_i(\bar{s}_l,p)\\ r_{3i}y_i(\bar{s}_l,p)\end{bmatrix} + \frac{1}{n}\sum_{l=0}^{n}\lambda_l\sum_{i=1}^{3}\begin{bmatrix}\bar{k}_{1i}(\bar{s}_l,\bar{x}_m,p)y_i(\bar{s}_l,p)\\ \bar{k}_{2i}(\bar{s}_l,\bar{x}_m,p)y_i(\bar{s}_l,p)\\ \bar{k}_{3i}(\bar{s}_l,\bar{x}_m,p)y_i(\bar{s}_l,p)\end{bmatrix} = -\begin{bmatrix}\sigma_0\\ D_0-D_0^c\\ B_0-B_0^c\end{bmatrix}, \tag{45}$$

where $m=1,2,\ldots,n$.

Moreover, the single-value conditions $u_z(a,0,t)=\phi(a,0,t)=\varphi(a,0,t)=0$ and $u_z(c,0,t)=\phi(c,0,t)=\varphi(c,0,t)=0$ give

$$\int_a^c g_i(x,p)dx = 0, \quad i=1,2,3, \tag{46}$$

which can be discretized as

$$\sum_{l=0}^{n}\lambda_l y_i(\bar{s}_l,p) = 0, \quad i=1,2,3. \tag{47}$$

Clearly, Eqs. (45) and (47) form a system of linear algebraic equations. However, it is found that the numbers of the unknowns and equations in the linear system are $3n+5$ and $3n+3$, respectively. In order to uniquely determine the unknowns, two other independent equations are needed, which can be given by two semi-permeable electric and magnetic boundary conditions at the crack faces. Note that when the crack-face magnetoelectric boundary conditions are four ideal cases: electro-magnetically permeable, electro-magnetically impermeable, electrically impermeable and magnetically permeable, electrically permeable and magnetically impermeable, the linear system can be solved directly. For a general semi-permeable assumption, the electric displacement D_0^c and magnetic induction B_0^c are still unknowns dependent on the unknowns to be determined, so the relevant equations are nonlinear, which are given in the next section.

4. Magnetoelectric field inside the cracks

To obtain the solutions of electric displacement D_0^c and magnetic induction B_0^c inside the dielectric crack, the Laplace transform (19) is applied to (12), and we have

$$D_0^c\Delta u_z^*(x,0,p) = -\varepsilon_r\varepsilon_0\Delta\phi^*(x,0,p), \tag{48}$$

$$B_0^c\Delta u_z^*(x,0,p) = -\mu_r\mu_0\Delta\varphi^*(x,0,p). \tag{49}$$

In view of (30), Eqs. (48) and (49) can be further rewritten as

$$D_0^c\int_x^c g_1(s,p)ds = -\varepsilon_r\varepsilon_0\int_x^c g_2(s,p)ds, \quad a<x<c, \tag{50}$$

$$B_0^c\int_x^c g_1(s,p)ds = -\mu_r\mu_0\int_x^c g_3(s,p)ds, \quad a<x<c. \tag{51}$$

Then taking into account (39) and (42), the above results reduce to

$$D_0^c \int_{\bar{x}}^{1} \frac{y_1(\bar{s},p)}{\sqrt{1-\bar{s}^2}} d\bar{s} = -\varepsilon_r \varepsilon_0 \int_{\bar{x}}^{1} \frac{y_2(\bar{s},p)}{\sqrt{1-\bar{s}^2}} d\bar{s}, \quad -1 < \bar{x} < 1, \tag{52}$$

$$B_0^c \int_{\bar{x}}^{1} \frac{y_1(\bar{s},p)}{\sqrt{1-\bar{s}^2}} d\bar{s} = -\mu_r \mu_0 \int_{\bar{x}}^{1} \frac{y_3(\bar{s},p)}{\sqrt{1-\bar{s}^2}} d\bar{s}, \quad -1 < \bar{x} < 1. \tag{53}$$

Similar to the observations given by Hao and Shen (1994) and Li and Lee (2004) for the electric displacement of crack interior, it is found from Zhong and Li (2007) that the electric displacement and magnetic induction inside the opening crack are constants and dependent on applied magneto-electro-elastic loads, material properties, dielectric permittivity and magnetic permeability of crack interior. The geometry of cracks does not affect their values, details of which are given in Appendix B. In other words, based on the Lobatto–Chebyshev quadrature technique, Eqs. (52) and (53) can be discretized when $\bar{x} = 0$ as

$$D_0^c \sum_{l=0}^{n/2} \lambda_l y_1(\bar{s}_l,p) + \varepsilon_r \varepsilon_0 \sum_{l=0}^{n/2} \lambda_l y_2(\bar{s}_l,p) = 0, \tag{54}$$

$$B_0^c \sum_{l=0}^{n/2} \lambda_l y_1(\bar{s}_l,p) + \mu_r \mu_0 \sum_{l=0}^{n/2} \lambda_l y_3(\bar{s}_l,p) = 0, \tag{55}$$

where n is chosen as an even number.

Obviously, Eqs. (45) and (47) together with (54) and (55) form a nonlinear system of $3n+5$ polynomial equations which can be solved efficiently by a homotopy continuation method (Li et al., 1987). Moreover, here let us rewrite the linear system made of (45) and (47) as

$$\mathbf{R}_{(3n+3)\times(3n+3)} \cdot \mathbf{Y} = \mathbf{S}, \tag{56}$$

or

$$\mathbf{Y} = \mathbf{R}^{-1}_{(3n+3)\times(3n+3)} \cdot \mathbf{S}, \tag{57}$$

where $\mathbf{R}_{(3n+3)\times(3n+3)}$ is the coefficient matrix and nonsingular. $\mathbf{Y}$ and $\mathbf{S}$ denote the vectors given as follows, respectively:

$$\mathbf{Y} = [y_1(\bar{s}_0,0,p),\ldots,y_1(\bar{s}_n,0,p),y_2(\bar{s}_0,0,p),\cdots, y_2(\bar{s}_n,0,p),y_3(\bar{s}_0,0,p),\ldots,y_3(\bar{s}_n,0,p)]^T, \tag{58}$$

$$\mathbf{S} = -\left[\underbrace{\sigma_0,\ldots,\sigma_0}_{n},\underbrace{D_0-D_0^c,\cdots,D_0-D_0^c}_{n},\underbrace{B_0-B_0^c,\ldots,B_0-B_0^c}_{n},0,0,0\right]^T, \tag{59}$$

where superscript "T" stands for transposition. Substituting (57) into (54) and (55), one can obtain

$$\mathbf{X_D} \cdot \mathbf{R}^{-1}_{(3n+3)\times(3n+3)} \cdot \mathbf{S} = 0, \tag{60}$$

$$\mathbf{X_B} \cdot \mathbf{R}^{-1}_{(3n+3)\times(3n+3)} \cdot \mathbf{S} = 0, \tag{61}$$

where

$$\mathbf{X_D} = \left[\underbrace{\lambda_0 D_0^c,\ldots,\lambda_{n/2} D_0^c}_{1+n/2},\underbrace{0,\ldots,0}_{n/2},\underbrace{\lambda_0 \varepsilon_r \varepsilon_0,\ldots,\lambda_{n/2}\varepsilon_r\varepsilon_0}_{1+n/2},\underbrace{0,\ldots,0}_{n/2+n+1}\right], \tag{62}$$

$$\mathbf{X_B} = \left[\underbrace{\lambda_0 B_0^c,\ldots,\lambda_{n/2} B_0^c}_{1+n/2},\underbrace{0,\ldots,0}_{n/2+n+1},\underbrace{\lambda_0 \mu_r \mu_0,\ldots,\lambda_{n/2}\mu_r\mu_0}_{1+n/2},\underbrace{0,\ldots,0}_{n/2}\right]. \tag{63}$$

From (60) and (61), two coupled quadric equations with respect to D_0^c and B_0^c are determined, which have at most four-pairs roots. Among these candidate solutions, only one pair of D_0^c and B_0^c are reasonable and the others are superfluous. An accepted pair of D_0^c and B_0^c can be chosen by considering that the magnetoelectric field inside the crack should be located at the range between that for an electro-magnetically impermeable crack and that for an electro-magnetically permeable one, or $\Delta u_z(x,0,t) \geqslant 0$ should be satisfied (Zhong and Li, 2007). For a special magnetoelectric material whose relevant properties are given in Table 1 (Tian and Rajapakse, 2005), Figs. 2 and 3 are depicted to show the variations of D_0^c and B_0^c on applied electric loading $\lambda_d = D_0 c_{33}/\sigma_0 e_{33}$ and magnetic loading $\lambda_b = B_0 c_{33}/\sigma_0 h_{33}$, respectively. For simplicity, hereafter it is assumed that $\sigma_0 = 10$ MPa and $\varepsilon_r = \mu_r$. As shown in Fig. 2, when $\varepsilon_r = \mu_r = 0$, meaning that the crack is electro-magnetically impermeable, it is seen that the electric displacement D_0^c is equal to zero. When $\varepsilon_r = \mu_r = \infty$, corresponding to an electro-magnetically permeable crack, D_0^c has a linear relation with λ_d. For a general case with an electromagnetical dielectric inside the crack, one can see that the curves of D_0^c increase with rising λ_d, and are situated between that for a fully permeable crack and that for a fully impermeable crack. The similar phenomena can be observed in Fig. 3 for the variations of magnetic induction B_0^c versus λ_d. The above results reveal that four ideal crack-face electromagnetic boundary conditions are indeed the limiting cases of the proposed general one.

Once D_0^c and B_0^c are determined and inserted into the linear system of (45) and (47), the other unknowns can be calculated. Furthermore, the magnetoelectroelastic field near the crack tips can be obtained.

Table 1
The relevant material properties.

c_{11}	c_{13}	c_{33}	c_{44}	e_{31}	e_{33}	e_{15}	h_{31}
226	124	216	44	−2.2	9.3	5.8	290.2
h_{33}	h_{15}	ε_{11}	ε_{33}	μ_{11}	μ_{33}	d_{11}	d_{33}
350	275	56.4	63.5	297	83.5	5.367	2737.5

Units: elastic stiffness constant, GPa; piezoelectric constants, C/m^2; piezomagnetic constants, N/Am; dielectric permittivities, ($\times 10^{-10}$) C^2/Nm^2; magnetic permeabilities, ($\times 10^{-6}$) Ns^2/C^2; electromagnetic constants, ($\times 10^{-12}$) Ns/VC.

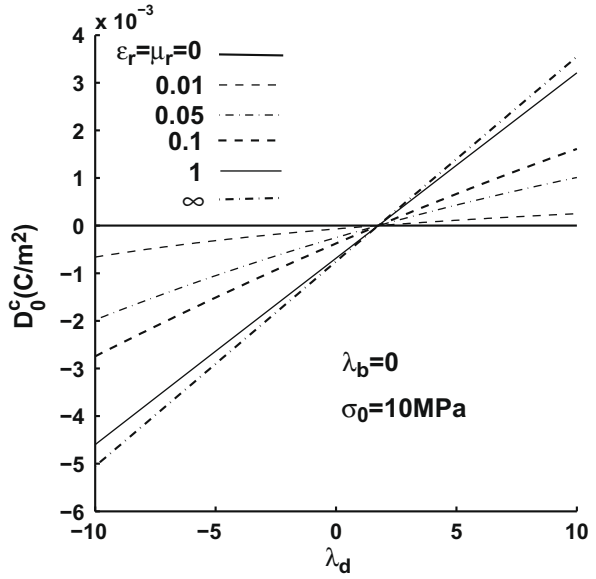

Fig. 2. The variations of D_0^c on λ_d with $\lambda_b = 0$ and $\sigma_0 = 10$ MPa for $\varepsilon_r = \mu_r = 0, 0.01, 0.05, 0.1, 1, \infty$, respectively.

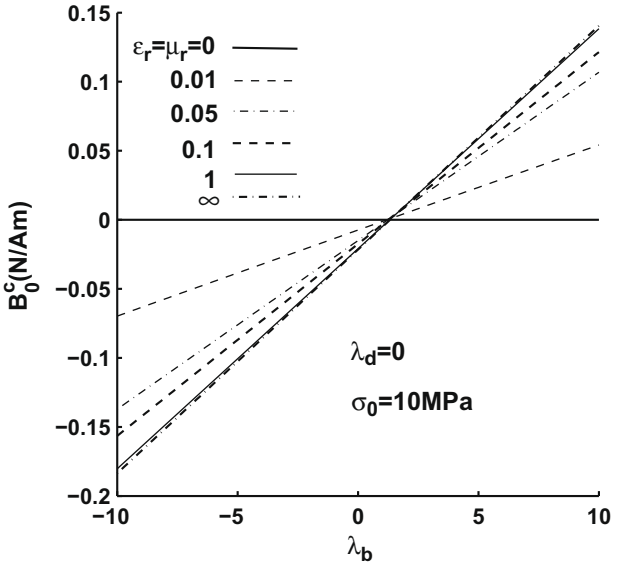

Fig. 3. The variations of B_0^c on λ_b with $\lambda_d = 0$ and $\sigma_0 = 10$ MPa for $\varepsilon_r = \mu_r = 0, 0.01, 0.05, 0.1, 1, \infty$, respectively.

5. Dynamic intensity factors

Of much importance are the dynamic intensity factors from the viewpoint of fracture mechanics which are usually utilized to characterize the crack tip field. Here we define the dynamic intensity factors of stress, electric displacement and magnetic induction near the inner and outer crack tips in the Laplace transform domain as follows:

$$K_{\text{inn}}^{q*} = \lim_{x\to a^-} \sqrt{2\pi(a-x)}\, q(x,0,p),$$
$$K_{\text{out}}^{q*} = \lim_{x\to c^+} \sqrt{2\pi(x-c)}\, q(x,0,p), \tag{64}$$

where $q(x,0,p)$ stands for one among $\sigma_{zz}^*(x,0,p)$, $D_z^*(x,0,p)$ and $B_z^*(x,0,p)$. From (25), after some computation, we arrive at

$$\begin{bmatrix} K_{\text{inn}}^{\sigma*} \\ K_{\text{inn}}^{D*} \\ K_{\text{inn}}^{B*} \end{bmatrix} = \frac{\sqrt{\pi a_0}}{p} \begin{bmatrix} r_{11} & r_{12} & r_{13} \\ r_{21} & r_{22} & r_{23} \\ r_{31} & r_{32} & r_{33} \end{bmatrix} \begin{bmatrix} y_1(-1,p) \\ y_2(-1,p) \\ y_3(-1,p) \end{bmatrix}, \tag{65}$$

near the inner crack tip, and

$$\begin{bmatrix} K_{\text{out}}^{\sigma*} \\ K_{\text{out}}^{D*} \\ K_{\text{out}}^{B*} \end{bmatrix} = -\frac{\sqrt{\pi a_0}}{p} \begin{bmatrix} r_{11} & r_{12} & r_{13} \\ r_{21} & r_{22} & r_{23} \\ r_{31} & r_{32} & r_{33} \end{bmatrix} \begin{bmatrix} y_1(1,p) \\ y_2(1,p) \\ y_3(1,p) \end{bmatrix}, \tag{66}$$

near the outer crack tip, where the factor $1/p$ is kept by virtue of (39).

On the other hand, the crack opening displacement is also an important fracture parameter to predict the crack growth in magnetoelectroelastic materials (Feng et al., 2007; Li and Lee, 2004). From the obtained results, one can express the crack opening displacements in the Laplace transform domain near the inner and outer crack tips as

$$\Delta u_z^{\text{inn}*}(x,0,p) = \frac{2a_0}{p} \int_{-1}^{\bar{x}} \frac{y_1(\bar{s},p)}{\sqrt{1-\bar{s}^2}} d\bar{s}, \tag{67}$$

$$\Delta u_z^{\text{out}*}(x,0,p) = -\frac{2a_0}{p} \int_{\bar{x}}^{1} \frac{y_1(\bar{s},p)}{\sqrt{1-\bar{s}^2}} d\bar{s}. \tag{68}$$

Furthermore, if defining the COD intensity factors near both crack tips as

$$K_{\text{inn}}^{\text{COD}*} = \lim_{x\to a^+} \frac{1}{2}\sqrt{\frac{\pi}{2(x-a)}}\, \Delta u_z^{\text{inn}*}(x,0,p), \tag{69}$$

$$K_{\text{out}}^{\text{COD}*} = \lim_{x\to c^-} \frac{1}{2}\sqrt{\frac{\pi}{2(c-x)}}\, \Delta u_z^{\text{out}*}(x,0,p), \tag{70}$$

we have

$$K_{\text{inn}}^{\text{COD}*} = \frac{\sqrt{\pi a_0}}{p} y_1(-1,p), \quad K_{\text{out}}^{\text{COD}*} = -\frac{\sqrt{\pi a_0}}{p} y_1(1,p). \tag{71}$$

In the end, the dynamic intensity factors of stress, electric displacement, magnetic induction and the COD can be determined in time domain by applying an inversion of the Laplace transform.

6. Numerical results and discussions

In order to illustrate the influences of the dielectric permeability of crack interior, applied loadings and the geometry of the crack on the dynamic intensity factors, numerical computations are carried out for a special magnetoelectroelastic material (Tian and Rajapakse, 2005). The values of r_{ki} appearing in (35) are evaluated as follows:

$$\begin{bmatrix} r_{11} & r_{12} & r_{13} \\ r_{21} & r_{22} & r_{23} \\ r_{31} & r_{32} & r_{33} \end{bmatrix} = \begin{bmatrix} 7.32556\times10^{10} & 5.52745 & 157.9328 \\ 5.52745 & -6.3327\times10^{-9} & -9.0099\times10^{-9} \\ 157.9328 & -9.0099\times10^{-9} & -1.5807\times10^{-4} \end{bmatrix}. \tag{72}$$

Moreover, to perform the Laplace inversion, the method proposed by Stehfest (1970) is used. That is, a numerical inversion $\varsigma(\pm1,t)$ of the Laplace transform $\Omega(\pm1,p)$ can be determined through

$$\varsigma(\pm1,t) \simeq \frac{\ln(2)}{t} \sum_{n=1}^{2N} V_n \Omega\left(\pm1, \frac{n\ln(2)}{t}\right), \tag{73}$$

with

$$V_n = (-1)^{n+N} \sum_{m=[(n+1)/2]}^{\min(n,N)} \frac{m^N(2m)!}{(N-m)!m!(m-1)!(n-m)!(2m-n)!}, \tag{74}$$

where $[(n+1)/2]$ is the integer part of the real number $(n+1)/2$. For simplicity, three typical crack models: impermeable (abbreviated for: electro-magnetically impermeable), vacuum and permeable (abbreviated for: electro-magnetically permeable) are only considered, and applied mechanical impact σ_0 is chosen as 10 MPa. In what follows, we investigate the variations of the dynamic intensity factors of stress and COD, that is, $\Omega(\pm1,p)$ stands for the numerical results of $K^{\sigma*}$ or $K^{\text{COD}*}$ at both tips by solving the resulting equations with the aid of the Lobatto–Chebyshev collocation method, and $\varsigma(\pm1,t)$ stands for the corresponding intensity factor K^{σ} or K^{COD} at both tips in the time domain.

For combined electromagnetic impacts $\lambda_d = 5$ and $\lambda_b = 10$, Figs. 4 and 5 are drawn to show the variations of the normalized intensity factors of stress and COD on the normalized time $c_s t/a_0$ with a special geometry of crack $c_0/a_0 = 1.2$ for three typical crack models, where $c_s = \sqrt{c_{44}/\rho}$. It is found from Fig. 4 that the curves of $K^{\sigma}/\sigma_0\sqrt{\pi a_0}$ exhibit the transient characteristic as usual (see, e.g. Li, 2005), regardless of the crack being impermeable, vacuum or permeable. Furthermore, the curves of $K^{\sigma}/\sigma_0\sqrt{\pi a_0}$ for a vacuum crack lie between that for an impermeable one and that for a permeable one, implying that the electro-magnetically impermeable and permeable crack models are the limiting cases of a dielectric crack. It is in accordance with the observations shown in Wang et al. (2008) and Zhong and Li (2007) for the exact analysis of static dielectric penny-shaped crack and Griffith one in a magnetoelectroelastic material. When $t \to \infty$, one can see from Fig. 4 that the curves of $K^{\sigma}/\sigma_0\sqrt{\pi a_0}$ near both the inner and outer crack tips tend

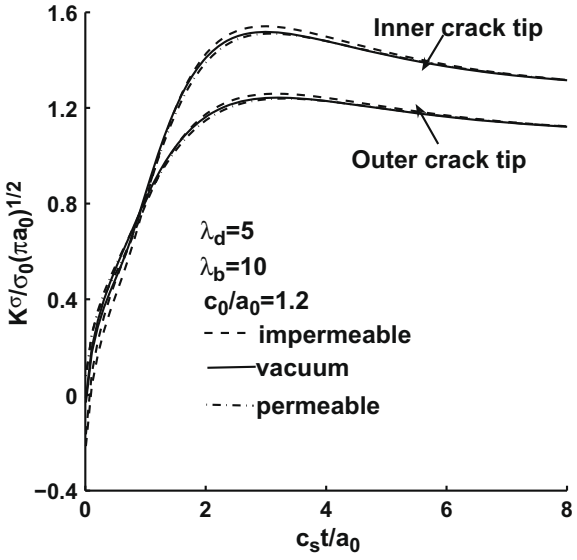

Fig. 4. The variations of $K^\sigma/\sigma_0\sqrt{\pi a_0}$ on $c_s t/a_0$ with electromagnetic impacts $\lambda_d = 5$ and $\lambda_b = 10$ for $c_0/a_0 = 1.2$ and three typical crack models, respectively.

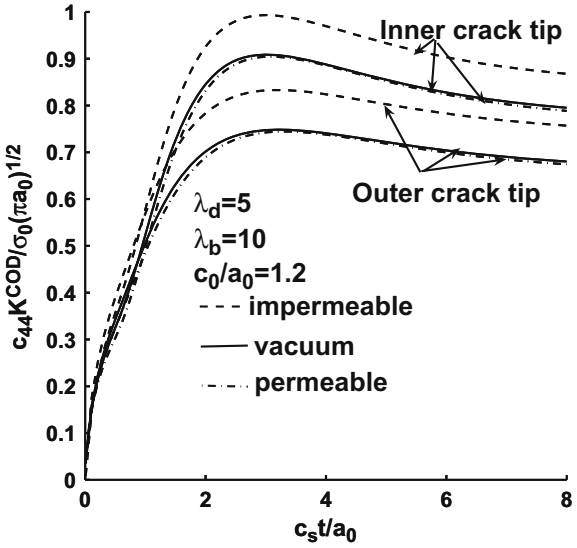

Fig. 5. The variations of $c_{44}K^{\mathrm{COD}}/\sigma_0\sqrt{\pi a_0}$ on $c_s t/a_0$ with electromagnetic impacts $\lambda_d = 5$ and $\lambda_b = 10$ for $c_0/a_0 = 1.2$ and three typical crack models, respectively.

to two constant values, respectively. The phenomena reveal that stress intensity factors are independent of the dielectric permittivity and magnetic permeability inside the crack, which is in agreement with the results given by Zhong and Li (2007) and Wang and Mai (2007) for a static state. Moreover, for a two collinear cracks, the peak value of $K^\sigma/\sigma_0\sqrt{\pi a_0}$ near the inner crack tip is larger than that near the outer crack tip. In addition, the similar observations can be also found in Fig. 5 where the variations of the normalized COD intensity factors versus the normalized time are depicted for three typical crack models. Furthermore, comparisons between Figs. 4 and 5 show that the dynamic stress intensity factors will be less than zero for $t \to 0$ when the crack is electromagnetically impermeable and vacuum. While the dynamic COD intensity factors are always greater than zero irrespective of the crack being impermeable, vacuum or permeable, implying that the COD intensity factor is more suitable to be a fracture criterion than the stress intensity factor for the dynamic crack growth of magnetoelectroelastic material (Feng et al., 2007; Peng and Li, 2009). As expected, the dynamic COD intensity factor near the inner crack tip is larger than that near the outer crack tip, meaning that the inner crack tip is easier to grow than the outer crack tip.

In what follows, let us focus on the effects of applied electromagnetic impacts on the dynamic intensity factors of stress and COD for a vacuum crack. In Fig. 6, the variations of $K^\sigma/\sigma_0\sqrt{\pi a_0}$ on $c_s t/a_0$ are presented with $\lambda_b = 0$ and $c_0/a_0 = 1.2$ for $\lambda_d = 50, 0, -50$, respectively. It is found from Fig. 6 that applied positive electric loading enhances the peak value of the dynamic intensity factor, and applied negative one decreases the peak value of the dynamic intensity factor. It is similar to the observations given in Li (2005) for the case of electro-magnetically impermeable crack, and different from the results shown by Yong and Zhou (2007) where electromagnetically permeable crack model is used. Moreover, when $t \to +\infty$, the curves of $K^\sigma/\sigma_0\sqrt{\pi a_0}$ near both crack tips tend to identical values, respectively, implying that the stress intensity factor is independent of applied electric loadings for a static state, which is in accordance with the known results (Zhong and Li, 2007). Furthermore, the effects of applied electric loadings on the normalized dynamic COD intensity factor are shown in Fig. 7. One can see that

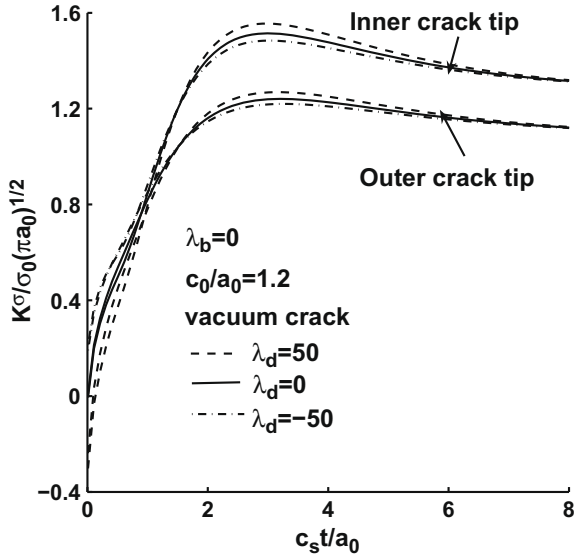

Fig. 6. The variations of $K^\sigma/\sigma_0\sqrt{\pi a_0}$ on $c_s t/a_0$ for a vacuum crack with $\lambda_b = 0$, $c_0/a_0 = 1.2$ and $\lambda_d = 50, 0, -50$, respectively.

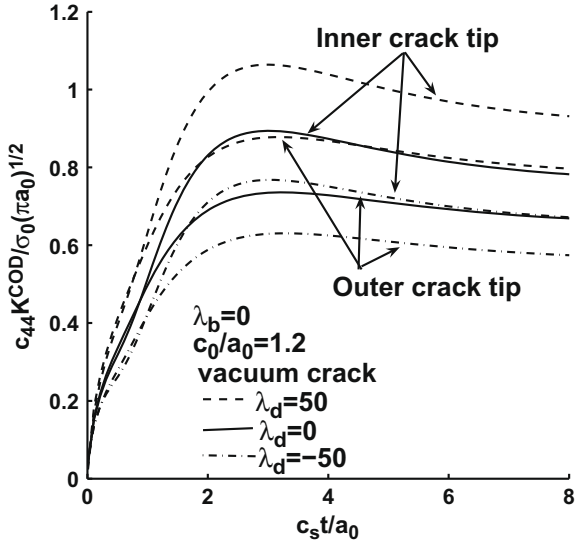

Fig. 7. The variations of $c_{44}K^{\mathrm{COD}}/\sigma_0\sqrt{\pi a_0}$ on $c_s t/a_0$ for a vacuum crack with $\lambda_b = 0$, $c_0/a_0 = 1.2$ and $\lambda_d = 50, 0, -50$, respectively.

positive electric field increases the dynamic COD intensity factor, and negative one decreases the dynamic COD intensity factor. The obtained results reveal that positive electric field enhances the crack growth, and negative one retards the crack growth for the dynamic dielectric crack of magnetoelectroelastic materials. This is in agreement with the experimental results given by Park and Sun (1995) for the effects of electric field on the crack growth in piezoelectric materials. In addition, the similar observations can be found for the influences of applied magnetic loadings on dynamic intensity factors of stress and COD, and the corresponding figures are neglected here.

In the end, the influences of the crack geometry on the dynamic stress and COD intensity factors are investigated and shown in Figs. 8 and 9, respectively. Under the combined electromagnetic impacts $\lambda_d = 5$ and $\lambda_b = 10$, it is seen from Figs. 8 and 9 that the values of the dynamic stress and COD intensity factors near the inner and outer crack tips rise with decreasing c_0/a_0, that is, the smaller the distance between two dielectric cracks, the greater the dynamic intensity factors of stress and COD. The observed results show that the distance of two dielectric cracks is smaller, the crack is easier to propagate, which is similar to the usual observations for two collinear cracks embedded in a magnetoelectroelastic material (Zhou et al., 2007).

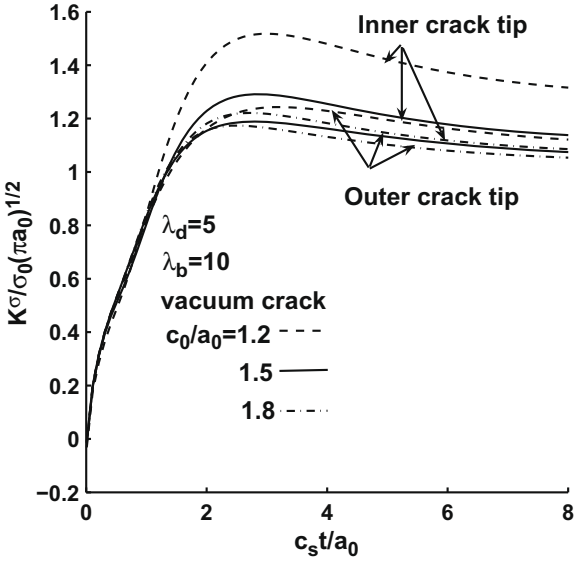

Fig. 8. The variations of $K^\sigma/\sigma_0\sqrt{\pi a_0}$ on $c_s t/a_0$ for a vacuum crack with $\lambda_d = 5$, $\lambda_b = 10$ and $c_0/a_0 = 1.2, 1.5, 1.8$, respectively.

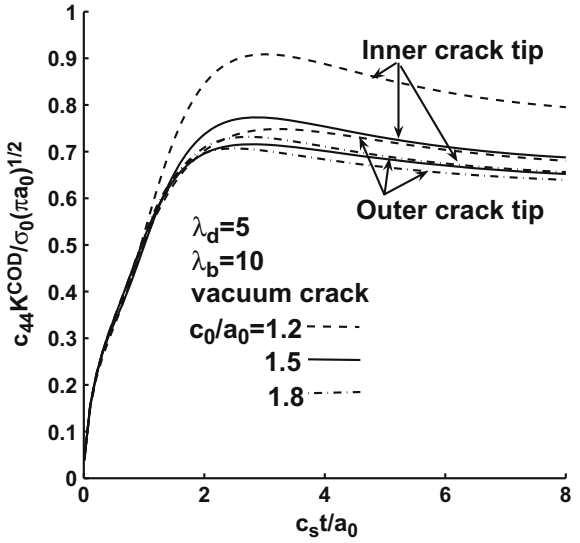

Fig. 9. The variations of $c_{44}K^{COD}/\sigma_0\sqrt{\pi a_0}$ on $c_s t/a_0$ for a vacuum crack with $\lambda_d = 5$, $\lambda_b = 10$ and $c_0/a_0 = 1.2, 1.5, 1.8$, respectively.

7. Conclusions

The problem of two collinear electro-magnetically dielectric cracks embedded in a magnetoelectroelastic material is considered under sudden magneto-electro-mechanical impacts. General crack-face electromagnetic boundary conditions are used to simulate realistic opening cracks. Applying the Fourier and Laplace transforms, the mixed-initial-value boundary problem is reduced to singular integral equations with Cauchy kernel. The dynamic intensity factors of stress, electric displacement, magnetic induction and the COD are obtained in time domain by an inversion of the Laplace transform. Numerical results are calculated for a special magnetoelectroelastic material to show the effects of dielectric inside the cracks, applied electromagnetic impacts and the crack geometry on the fracture parameters. Some observations are drawn out as follows:

- Four ideal crack-face electromagnetic boundary conditions are the limiting cases of the electro-magnetically dielectric crack model.
- The COD intensity factor is suitable as a fracture criterion for a dynamic electro-magnetically dielectric crack in a magnetoelectroelastic solid.
- Positive electromagnetic impact loadings enhance the dynamic electro-magnetically dielectric crack propagation, and negative electromagnetic ones retard the dynamic electro-magnetically dielectric crack growth.
- For two collinear dielectric cracks under the dynamic loadings, the inner crack tip is easier to propagate than the outer crack tip, and the smaller the distance between two cracks, the easier crack growth.

Acknowledgments

X.-F.L. acknowledges the supports from the National Natural Science Foundation of China (Grant No. 10672189). X.-C.Z. appreciates the supports from the Scientific Research Foundation of Guangxi University (X081088). The authors would like to give their thanks to two anonymous reviewers for valuable comments and suggestions on an earlier version of this paper.

Appendix A

$\alpha_j(\xi, p)$ appearing in (24) are the roots of the following characteristic equation

$$\begin{vmatrix} c_{11}\xi^2+\rho p^2-c_{44}\alpha^2 & -(c_{13}+c_{44})\alpha\xi & -(e_{31}+e_{15})\alpha\xi & -(h_{31}+h_{15})\alpha\xi \\ -(c_{13}+c_{44})\alpha\xi & c_{33}\alpha^2-c_{44}\xi^2-\rho p^2 & e_{33}\alpha^2-e_{15}\xi^2 & \alpha^2 h_{33}-h_{15}\xi^2 \\ -(e_{31}+e_{15})\alpha\xi & e_{33}\alpha^2-e_{15}\xi^2 & \varepsilon_{11}\xi^2-\varepsilon_{33}\alpha^2 & d_{11}\xi^2-d_{33}\alpha^2 \\ -(h_{31}+h_{15})\alpha\xi & h_{33}\alpha^2-h_{15}\xi^2 & d_{11}\xi^2-d_{33}\alpha^2 & \mu_{11}\xi^2-\mu_{33}\alpha^2 \end{vmatrix} = 0, \tag{A1}$$

and $Re[\alpha_j(\xi, p)] > 0$ should be hold to ensure the convergence of the physical quantities for $z \to \infty$. Moreover, η_{3j}, η_{4j} and η_{5j} can be determined by

$$\alpha_j^2(\xi,p)=\frac{c_{11}\xi^2+\rho p^2}{c_{44}+(c_{13}+c_{44})\eta_{3j}\xi+(e_{31}+e_{15})\eta_{4j}\xi+(h_{31}+h_{15})\eta_{5j}\xi}$$
$$=\frac{(c_{13}+c_{44})\xi+(c_{44}\xi^2+\rho p^2)\eta_{3j}+e_{15}\xi^2\eta_{4j}+h_{15}\xi^2\eta_{5j}}{c_{33}\eta_{3j}+e_{33}\eta_{4j}+h_{33}\eta_{5j}}$$
$$=\frac{(e_{31}+e_{15})\xi+(e_{15}\eta_{3j}-\varepsilon_{11}\eta_{4j}-d_{11}\eta_{5j})\xi^2}{e_{33}\eta_{3j}-\varepsilon_{33}\eta_{4j}-d_{33}\eta_{5j}}$$
$$=\frac{(h_{31}+h_{15})\xi+(h_{15}\eta_{3j}-d_{11}\eta_{4j}-\mu_{11}\eta_{5j})\xi^2}{h_{33}\eta_{3j}-d_{33}\eta_{4j}-\mu_{33}\eta_{5j}}. \tag{A2}$$

The functions β_{ij} $(i=0,1,2,3)$ appearing in (25) are determined as

$$\beta_{0j}=[c_{44}(1+\eta_{3j}\xi)+e_{15}\eta_{4j}\xi+h_{15}\eta_{5j}\xi]\alpha_j, \tag{A3}$$
$$\beta_{1j}=(c_{33}\eta_{3j}+e_{33}\eta_{4j}+h_{33}\eta_{5j})\alpha_j^2-c_{13}\xi, \tag{A4}$$
$$\beta_{2j}=(e_{33}\eta_{3j}-\varepsilon_{33}\eta_{4j}-d_{33}\eta_{5j})\alpha_j^2-e_{31}\xi, \tag{A5}$$
$$\beta_{3j}=(h_{33}\eta_{3j}-d_{33}\eta_{4j}-\mu_{33}\eta_{5j})\alpha_j^2-h_{31}\xi. \tag{A6}$$

Appendix B

Noting that the electric displacement D_0^c and magnetic induction B_0^c inside the cracks are independent of time, they can be solved under the action of static loadings σ_0, D_0 and B_0. Thus for the static problem of two collinear dielectric cracks in a magneto-electroelastic solid, the functions α_j, $\beta_{\kappa j}$ $(\kappa=0,1,2,3)$, η_{ij} $(i=3,4,5)$ become constants dependent on the material properties only. Similar to Zhong and Li (2007), application of the boundary conditions (9)–(16) yields the following coupling equations:

$$\sum_{j=1}^{4}\beta_{0j}A_j(\xi)=0, \tag{B1}$$

$$\sum_{j=1}^{4}\left[D_0^c\eta_{3j}+\varepsilon^c\eta_{4j}\right]\alpha_jA_j(\xi)=0,\quad \sum_{j=1}^{4}\left[B_0^c\eta_{3j}+\mu^c\eta_{5j}\right]\alpha_jA_j(\xi)=0, \tag{B2}$$

$$\sum_{j=1}^{4}[(D_0-D_0^c)\beta_{1j}-\beta_{2j}\sigma_0]A_j(\xi)=0,\quad \sum_{j=1}^{4}[(B_0-B_0^c)\beta_{1j}-\beta_{3j}\sigma_0]A_j(\xi)=0. \tag{B3}$$

Clearly, D_0^c and B_0^c can be determined by solving the above system of algebraic equations and are found to depend on applied magneto-electro-elastic loadings, the material properties as well as the electric permittivity and magnetic permeability of crack interior. The geometry of two collinear cracks does not change D_0^c and B_0^c, which is in agreement with the observations given by Zhou et al. (2007) for two collinear cracks in a magnetoelectroelastic material and Hao (2001) for multiple collinear cracks in a piezoelectric solid.

References

Du, J.K., Shen, Y.P., Ye, D.Y., Yue, F.R., 2004. Scattering of anti-plane shear waves by a partially debonded magneto-electro-elastic circular cylindrical inhomogeneity. International Journal of Engineering Science 42, 887–913.

Feng, W.J., Pan, E., 2008. Dynamic fracture behavior of an internal interfacial crack between two dissimilar magneto-electro-elastic plates. Engineering Fracture Mechanics 75, 1468–1487.

Feng, W.J., Pan, E., Wang, X., 2007. Dynamic fracture analysis of a penny-shaped crack in a magnetoelectroelastic layer. International Journal of Solids and Structures 44, 7955–7974.

Gao, C.F., Tong, P., Zhang, T.Y., 2004. Fracture mechanics for a mode III crack in a magnetoelectroelastic solid. International Journal of Solids and Structures 41, 6613–6629.

Hao, T.H., 2001. Multiple collinear cracks in a piezoelectric material. International Journal of Solids and Structures 38, 9201–9208.

Hao, T.H., Shen, Z.Y., 1994. A new electric boundary condition of electric fracture mechanics and its application. Engineering Fracture Mechanics 47, 793–802.

Hu, K.Q., Li, G.Q., 2005a. Electro-magneto-elastic analysis of a piezoelectromagnetic strip with a finite crack under longitudinal shear. Mechanics of Materials 37, 925–934.

Hu, K.Q., Li, G.Q., 2005b. Constant moving crack in a magnetoelctroelastic material under anti-plane shear loading. International Journal of Solids and Structures 42, 2823–2835.

Hu, K.Q., Kang, Y.L., Li, G.Q., 2006. Moving crack at the interface between two dissimilar magnetoelectroelastic materials. Acta Mechanica 182, 1–16.

Hu, K.Q., Kang, Y.L., Qin, Q.H., 2007. A moving crack in a rectangular magnetoelectroelastic body. Engineering Fracture Mechanics 74, 751–770.

Li, X.-F., 2005. Dynamic analysis of a cracked magnetoelectroelastic medium under antiplane mechanical and inplane electric and magnetic impacts. International Journal of Solids and Structures 42, 3185–3205.

Li, X.F., Lee, K.Y., 2004. Crack growth in a piezoelectric material with a Griffth crack perpendicular to the poing axis. Philosophical Magazine 84, 1789–1820.

Li, T.Y., Sauer, T., Yorke, J.A., 1987. Numerical solution of a class of deficient polynomial systems. SIAM Journal of Numerical Analysis 24, 435–451.

Liu, J.X., Liu, X.L., Zhao, Y.B., 2001. Green's functions for anistropic magnetoelectroelastic solids with an elliptical cavity or a crack. International Journal of Engineering Science 39, 1405–1418.

McMeeking, R.M., 1999. Crack tip energy release rate for a piezoelectric compact tension specimen. Engineering Fracture Mechanics 47, 793–802.

Nan, C.W., Bichurin, M.I., Dong, S.X., et al., 2008. Multiferroic magnetoelectric composites: Historical perspective, status, and future directions. Journal of Applied Physics 103, 031101.

Park, S., Sun, C.T., 1995. Fracture criteria for piezoelectric ceramics. Jounal of Amercian Ceramic Society 78, 1475–1480.

Peng, X.-L., Li, X.-F., 2009. Transient response of the crack-tip field in a magnetoelectroelastic half-space with a functionally graded coating under impacts. Archive of Applied Mechanics. doi:10.1007/s00419-008-0277-7.

Schneider, G.A., Felten, F., McMeeking, R.M., 2003. The electrical potential difference across cracks in PZT measured by Kelvin Probe Microscopy and implications for fracture. Acta Materialia 51, 2235–2241.

Sih, G.C., Jones, R., Song, Z.F., 2003. Piezomagnetic and piezoelectric poling effects on modes I and II crack initiation behavior of magnetoelectroelastic materials. Theoretical and Applied Fracture Mechanics 40, 161–186.

Stehfest, H., 1970. Numerical inversion of Laplace transforms. Communications ACM 13 (47–49), 624.

Su, R.K.L., Feng, W.J., Liu, J., 2007. Transient response of interface cracks between dissimilar magneto-electro-elastic strips under out-of-plane mechanical and in-plane magneto-electrical impact loads. Composite Structures 78, 119–128.

Theocaris, P.S., Ioakimidis, N.I., 1977. Numerical integration methods for the solution of singular integral equations. Quarterly of Applied Mathematics 35, 173–183.

Tian, W.Y., Rajapakse, R.K.N.D., 2005. Fracture analysis of magnetoelectroelastic solids by using path independent integrals. International Journal of Fracture 131, 311–335.

Wang, B.L., Mai, Y.W., 2007. Applicability of the crack-face electromagnetic boundary conditions for fracture of magnetoelectroelastic materials. International Journal of Solids and Structures 44, 387–398.

Wang, B.L., Sun, Y.G., Zhang, H.Y., 2008. Analysis of a penny-shaped crack in magnetoelectroelastic materials. Journal of Applied Physics 103, 083530.

Yong, H.-D., Zhou, Y.H., 2007. Transient response of a cracked magnetoelectroelastic strip under anti-plane impact. International Journal of Solids and Structures 44, 705–717.

Zhao, M.H., Fan, C.Y., Yang, F., Liu, T., 2007. Analysis method of planar cracks of arbitrary shape in the isotropic plane of a three-dimensional transversely isotropic magnetoelectroelastic medium. International Journal of Solids and Structures 44, 4505–4523.

Zheng, H., Wang, J., Lofland, S.E., et al., 2004. Multiferroic $BaTiO_3$–$CoFe_2O_4$ nanostructures. Science 303, 661–663.

Zhong, X.-C., Li, X.-F., 2006. A finite length crack propagating along the interface of two dissimilar magnetoelectroelastic materials. International Journal of Engineering Science 44, 1394–1407.

Zhong, X.-C., Li, X.-F., 2007. Magnetoelectroelastic analysis for an opening crack in a piezoelectromagnetic solid. European Journal of Mechanics A 26, 405–417.

Zhong, X.-C., Li, X.-F., Lee, K.Y., 2009. Transient response of a cracked magnetoelectric material under the action of in-plane sudden impacts. Computational Materials Science. doi:10.1016/j.commatsci.2008.12.013.

Zhou, Z.G., Wu, L.Z., Wang, B., 2005. The dynamic behaviour of two collinear interfaces cracks in magneto-electro-elastic materials. European Journal of Mechanics A 24, 253–262.

Zhou, Z.G., Zhang, P.W., Wu, L.Z., 2007. Solutions to a limited-permeable crack or two limited-permeable collinear cracks in piezoelectric/piezomagnetic materials. Archive of Applied Mechanics 77, 861–882.